IEEE Access
Multidisciplinary ⋮ Rapid Review ⋮ Open Access Journal

Received 8 May 2024, accepted 10 June 2024, date of publication 12 June 2024, date of current version 21 June 2024.

Digital Object Identifier 10.1109/ACCESS.2024.3413577

RESEARCH ARTICLE

Design of a 2D/3D Positioning System and Its Real-Time Application With Low-Cost Sensors

SERKAN ZOBAR[1], MEHMET CIYDEM[1], ÖZGÜL SALOR[1,2], (Senior Member, IEEE), JIYONG KWAG[3,4], CHARLES K. TOTH[4], (Life Senior Member, IEEE), AND ALPER YILMAZ[4], (Senior Member, IEEE)

[1]Department of Electrical and Electronics Engineering, Gazi University, 06570 Ankara, Türkiye
[2]Department of Electrical and Electronics Engineering, Kyrgyz-Turkish Manas University, Bishkek 720044, Kyrgyzstan
[3]Center for Automotive Research, The Ohio State University, Columbus, OH 43212, USA
[4]Department of Civil, Environmental, and Geodetic Engineering, The Ohio State University, Columbus, OH 43210, USA

Corresponding author: Serkan Zobar (serkan.zobar@gazi.edu.tr)

This work was supported by the Scientific and Technological Research Council of Türkiye (TUBITAK) under Grant 1059B142100661.

ABSTRACT In this article, we introduce a positioning system developed for two- and three-dimensional motion tracking. The system is based on a recursive Bayesian estimator with a dynamic naive Bayesian classifier map matching scheme. The states of the dynamic naive Bayesian classifier are created by using the map information and partitioning the region of interest into grids. The developed positioning system considers three types of measurements of the platform at each time instant: the heading measurement to determine the prior probability distribution; the single-anchor distance and altitude measurements to determine the observation likelihood. A recursive Bayesian estimator takes advantage of these measurements to obtain the posterior probability distribution. Ultimately, via the obtained posterior probability distribution, the most probable projection of these measurements onto the states of the dynamic naive Bayesian classifier is estimated as the current position of the platform. To avoid the potential ambiguities in the estimation process, the estimator exploits a design parameter that characterizes the platform's maximum attainable speed. Simulations and real-time application results are given to illustrate the effectiveness of the developed system for positioning applications in two- and three-dimensional indoor and outdoor environments with constraints, such as corridors, roads, or flight paths.

INDEX TERMS Bayesian estimation, dynamic naive Bayesian classifier, map matching, maximum a posteriori, single-anchor positioning.

I. INTRODUCTION

Accurate and reliable two- or three-dimensional (2D or 3D) positioning of mobile platforms (e.g., pedestrians, unmanned ground vehicles, robots, drones, and autonomous underwater vehicles) is a very crucial task for a diverse set of applications emerging in both civilian and military areas [1]. Over the last three decades, Global Navigation Satellite Systems (GNSS) including GPS, Galileo, GLONASS, and Beidou have become the main technology for positioning purposes [2]. However, equipping mobile platforms with GNSS receivers provides an accurate and reliable positioning solution solely in outdoor environments where there is a clear and unobstructed view of the sky [3]. Therefore, research to develop alternative positioning systems that can be used in environments where GNSS signals are degraded or not accessible has gained a great deal of attention in both industry and academia [4], [5], [6], [7]. These environments include densely populated urban areas with skyscrapers and tall buildings, outdoor military operation areas affected by GNSS jamming or spoofing, indoor spaces, underground locations, etc. Each alternative positioning system suitable for these environments has its own set of advantages and drawbacks.

The associate editor coordinating the review of this manuscript and approving it for publication was Usama Mir.

© 2024 The Authors. This work is licensed under a Creative Commons Attribution-NonCommercial-NoDerivatives 4.0 License.
For more information, see https://creativecommons.org/licenses/by-nc-nd/4.0/

On one side, there are infrastructureless positioning systems, which rely solely on standalone sensing units, such as inertial accelerometers and gyroscopes, without any dependence on external preinstalled infrastructure in the environment. Their positioning strategy typically employs the dead reckoning approach, wherein the estimation of the platform's position relative to a starting point is derived from the motion data captured by inertial sensors. Despite achieving high precision over short durations, the dead reckoning positioning strategy experiences an unavoidable increase in drifting error as time elapses [8].

On the other side, there are infrastructure-based positioning systems that generally employ technologies such as radio frequency identification (RFID) [9], bluetooth low energy (BLE) [10], wireless fidelity (Wi-Fi) [11], ultra-wideband (UWB) [12], [13], and long range (LoRa) [14], offering distance measurements to obtain a positioning solution. These infrastructure-based positioning systems depend on preinstalled devices or facilities within the environment and vary in terms of accuracy, coverage, expenses related to deploying and maintaining, complexity of the system, and other factors. For example, RFID and BLE offer restricted range and positioning accuracies [15]. Wi-Fi positioning is cost-effective due to its utilization of existing infrastructures like public and private access points, yet it yields relatively low accuracy [16]. In contrast, UWB can attain accuracy at the centimeter level for distances of up to 290 m under line-of-sight (LoS) conditions [17], but the deployment of numerous UWB transceivers for extensive coverage incurs high costs. In scenarios requiring extended ranges and a broader coverage, LoRa offers distance estimations reaching up to 15 km [18].

To address the drawbacks briefly outlined for each system above and enhance positioning accuracy, integration of sensors and fusion of data become imperative [19]. For instance, to improve the long-term precision of dead reckoning, inertial sensors can be combined with additional sensors like magnetometers [20], barometers [21], and infrastructure-based systems including Wi-Fi [22] or UWB [23] technologies for the corrections of heading, altitude, and absolute position, respectively. Alongside sensor integration, fusing sensor data with available spatial information offers a favorable and cost efficient positioning solution, without the need for extra hardware. In practical applications, spatial data is presented using maps and floor plans. Map matching methods leverage spatial information to incorporate constraints within the navigational space, consequently enhancing positioning accuracy [24], [25]. Although numerous map matching-based methods have emerged recently, particle filter (PF)-based approaches remain dominant in map fusion research [26], [27], [28]. Nevertheless, PF-based methods face significant computational burdens and are susceptible to failure [29]. To alleviate the computational load of PF-based methods, a nonrecursive Bayesian map matching method is introduced in [30].

In our previous work [31], we developed a positioning system referred to as 2D-HASAP (two-dimensional heading-aided single-anchor positioning) which was utilizing the single-anchor distance and heading measurements of the mobile platform to obtain its 2D positioning estimate. The methodology of 2D-HASAP was solely demonstrated through simulations in [31].

The positioning system devised in this article is founded on the established research and methodology of 2D-HASAP, with the goal of attaining a more advanced and comprehensive positioning solution. To accomplish this goal, the following extensions and enhancements have been implemented:

- This article extends 2D-HASAP into 3D positioning, incorporating altitude measurements of the platform.
- This article introduces a dynamic naive Bayesian classifier (DNBC) [32] map matching scheme to handle multiple observed variables effectively, in contrast to the hidden Markov model (HMM) [33] map matching scheme employed by 2D-HASAP, which accounts for only a single observed variable.
- Alongside simulation studies, a real-time application was carried out to validate the performance of the developed positioning system in this article, and its results are presented.
- The developed positioning system in this article employs a recursive Bayesian estimator and encompasses two stages: motion and measurement updates. By taking into account the temporal relationship between the platform's current and previous positions through DNBC, maximum a posteriori inference is utilized to estimate the platform's current position.
- The developed positioning system in this article makes use of the heading measurement of the platform to compute the prior probability distribution. As a result, there is a notable decrease in the number of candidate states during DNBC map matching. This approach improves the computational efficiency of the developed positioning system.
- To compute the observation likelihood, the developed system in this article utilizes two measurements: the single-anchor distance (by the transmission of a limited number of messages between just two infrastructure-based transceivers, namely, one for the single anchor and one for the platform) and altitude measurements.
- All the measurements utilized by the developed positioning system in this article can be obtained from sensors that are highly efficient and cost-effective, resulting in a system with comparatively low cost and complexity.
- To address potential ambiguities arising during the probability projection of the measurements onto the states of DNBC, the developed positioning system in this article incorporates a design parameter characterizing the maximum speed that can be reached by the platform.

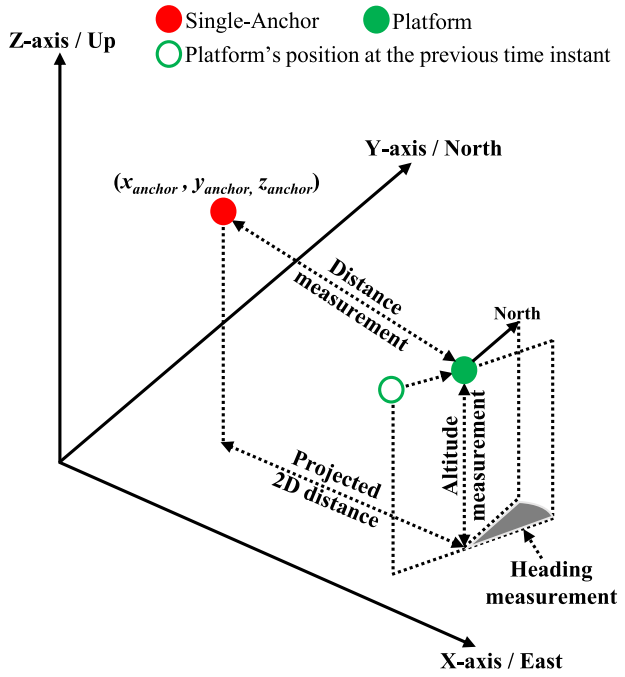

FIGURE 1. The measurements and the local coordinate system exploited by the developed positioning system.

The remaining sections of the article are structured as follows: Section II offers the detailed methodology of the developed positioning system. Simulations demonstrating the effectiveness of the developed positioning system are provided in Section III. The real-time application results are presented in Section IV. Finally, the article is concluded, and future research directions are given in Section V.

II. METHODOLOGY

In this section, a detailed description of the methodology used by the developed positioning system is presented. To provide an inclusive methodology description, the developed positioning system assumes that the platform moves in a 3D environment and the map information is complied with or converted to the local coordinate system as illustrated in Fig. 1. It is also assumed that the X-, Y-, and Z-axis of the coordinate system are aligned with the local east, north, and up directions, respectively. In addition, the developed positioning system has a preinstalled single anchor with specified position coordinates $(x_{anchor}, y_{anchor}, z_{anchor})$.

Furthermore, the developed system inherently offers a positioning solution for applications that rely on 2D maps by incorporating only two types of measurements: the heading and the projection of the single-anchor distance onto the XY plane as shown in Fig. 1.

A. MEASUREMENTS

The developed positioning system employs the platform's heading, single-anchor distance, and altitude measurements to determine its current position within a DNBC map matching scheme.

1) HEADING

The heading measurement of the platform represents the rotation from the local north direction within the range of $[-\pi, \pi)$ radian, with positive angles increasing eastward as depicted in Fig. 1. This measurement can be acquired using a digital compass, a gyroscope, or a combination of both. It is assumed that the orientation of these sensors is aligned with the platform's heading.

2) SINGLE-ANCHOR DISTANCE

The platform is presumed to have a transceiver such as UWB or LoRa for acquiring the measurement of its distance from a preinstalled single anchor with specified position coordinates $(x_{anchor}, y_{anchor}, z_{anchor})$ as shown in Fig. 1. The measured distance between the single-anchor and platform transceivers encompasses all measurement errors, including nonline-of-sight (NLoS) and multipath fading.

3) ALTITUDE

The altitude measurement provides information about the vertical distance of the platform above/below a fixed level. The platform altitude measurement can be obtained by using barometric altimeters, depth sensors, radar altimeters, etc.

B. DYNAMIC NAIVE BAYESIAN CLASSIFIER

DNBCs are a specialized form of Bayesian network, and can be considered as an extension of HMMs. DNBCs and HMMs vary in the number of observed variables; HMM defines only a single observed variable, while DNBC supports multiple observed variables. DNBCs are dynamic, because they classify sequences with variables at every time instant t_k. They are called naive, because the observed variables are assumed to be conditionally independent of each other. A DNBC is built upon the following assumptions:

- It has discrete hidden states.
- At time instant t_k, the hidden state is determined solely by the hidden state at time instant t_{k-1}, regardless of any states prior to t_{k-1}.
- At time instant t_k, multiple observations are produced by the hidden state which cannot be directly observed but can only be inferred through a probabilistic function.
- Observations at time instant t_k are unrelated to the hidden states and observations at any other time instants.
- Observations at time instant t_k are conditionally independent of each other.

Under these assumptions, the developed positioning system is founded on a DNBC featuring N hidden states, denoted as $\{c_1, c_2, \ldots, c_N\}$. These states correspond to potential discrete coordinates, indicating the platform's position as a grid cell on the map. The size of each grid cell, whether in 2D or 3D, impacts the quantity of hidden states N thereby influencing both the computational demands and accuracy of the positioning system. Larger cell sizes can lower computational costs but may compromise accuracy, while smaller sizes can enhance accuracy at the expense of increased computational load.

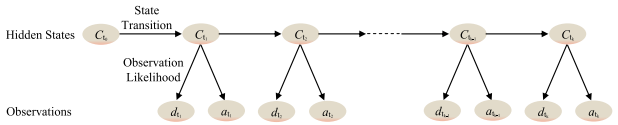

FIGURE 2. The developed positioning system utilizes a dynamic naive Bayesian classifier, an extension of hidden Markov models, to represent probability distributions across sequences of multivariate observations.

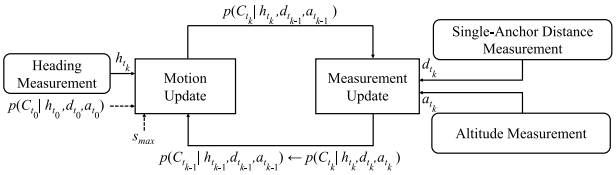

FIGURE 3. The iterative loop of the recursive Bayesian estimator used by the developed positioning system. The estimator comprises motion update via heading measurement and measurement update via single-anchor distance and altitude measurements.

The DNBC utilized by the developed positioning system has three measurement sequences, each comprising k measurements: $\{h_{t_1}, h_{t_2}, \ldots, h_{t_k}\}$, $\{d_{t_1}, d_{t_2}, \ldots, d_{t_k}\}$ and $\{a_{t_1}, a_{t_2}, \ldots, a_{t_k}\}$ which are the platform's heading, single-anchor distance, and altitude measurements, respectively, as shown in Fig. 2. The developed positioning system operates under the assumption that all measurements are acquired precisely as the platform arrives at the new position to be estimated during time instances t_l, $l = 1, 2, \ldots, k$.

The developed positioning system aims to update the posterior probability distribution $p(C_{t_k} = c_j|h_{t_k}, d_{t_k}, a_{t_k})$ to be in hidden state c_j at time instant t_k knowing the heading h_{t_k}, single-anchor distance d_{t_k}, and altitude a_{t_k} measurements at each time instant for each hidden state C_{t_k}. Utilizing this posterior probability distribution at time instant t_k, the position of the platform can be estimated using the maximum a posteriori inference scheme.

The posterior probability distribution, $p(C_{t_k} = c_j|h_{t_k}, d_{t_k}, a_{t_k})$, can be computed as given below:

$$p(C_{t_k} = c_j|h_{t_k}, d_{t_k}, a_{t_k}) = p(d_{t_k}, a_{t_k}|C_{t_k} = c_j) \cdot p(C_{t_k} = c_j|h_{t_k}, d_{t_{k-1}}, a_{t_{k-1}}). \quad (1)$$

As can be seen from (1), the posterior probability distribution $p(C_{t_k} = c_j|h_{t_k}, d_{t_k}, a_{t_k})$ can be recursively acquired through two sequential stages:

- Motion update providing the prior probability distribution $p(C_{t_k} = c_j|h_{t_k}, d_{t_{k-1}}, a_{t_{k-1}})$ and
- Measurement update providing the observation likelihood $p(d_{t_k}, a_{t_k}|C_{t_k} = c_j)$, also known as emission probability.

The iterative loop of the developed recursive Bayesian estimator above is depicted in Fig. 3.

C. MOTION UPDATE

During the motion update, we compute the prior probability distribution $p(C_{t_k} = c_j|h_{t_k}, d_{t_{k-1}}, a_{t_{k-1}})$ under the assumption that the platform's position c_j at time instant t_k is solely influenced by its previous position c_i at time instant t_{k-1} and the platform's heading measurement h_{t_k} at time instant t_k:

$$p(C_{t_k} = c_j|h_{t_k}, d_{t_{k-1}}, a_{t_{k-1}}) = \sum_{c_i} [p(C_{t_k} = c_j|C_{t_{k-1}} = c_i, h_{t_k}) \cdot p(C_{t_{k-1}} = c_i|h_{t_{k-1}}, d_{t_{k-1}}, a_{t_{k-1}})]. \quad (2)$$

Suppose that the posterior probability distribution $p(C_{t_{k-1}} = c_i|h_{t_{k-1}}, d_{t_{k-1}}, a_{t_{k-1}})$ for the hidden state c_i has been previously computed at time instant t_{k-1}, incorporating all measurements up to and including the time instant t_{k-1}.

The initial probability distribution, $p(C_{t_0}|h_{t_0}, d_{t_0}, a_{t_0})$, is assumed to be known and serves as the initial point for the recursive Bayesian estimation cycle, as depicted in Fig. 3. $p(C_{t_0}|h_{t_0}, d_{t_0}, a_{t_0})$ can be derived from a map-based starting point information. For instance, the platform can start to navigate from an exactly known position with pinpointed coordinates, i.e., $p(C_{t_0}|h_{t_0}, d_{t_0}, a_{t_0})$ is equal to 1 for the pinpointed coordinates, and 0 for all other coordinates. Alternatively, $p(C_{t_0}|h_{t_0}, d_{t_0}, a_{t_0})$ can be described in such a way that the uncertainties in the determination of the starting point are taken into account by the developed positioning system to initialize the recursive Bayesian estimation.

Provided the heading measurement h_{t_k} of the platform, the transition probability $p(C_{t_k} = c_j|C_{t_{k-1}} = c_i, h_{t_k})$ can be expressed as:

$$p(C_{t_k} = c_j|C_{t_{k-1}} = c_i, h_{t_k}) = \frac{p(h_{t_k}|C_{t_k} = c_j, C_{t_{k-1}} = c_i) \cdot p(C_{t_k} = c_j|C_{t_{k-1}} = c_i)}{p(h_{t_k}|C_{t_{k-1}} = c_i)}. \quad (3)$$

The probability distribution representing the heading measurement of the platform $p(h_{t_k}|C_{t_k} = c_j, C_{t_{k-1}} = c_i)$ in (3) is assumed to follow a wrapped normal distribution bounded within the range of $[-\pi, \pi)$ radian as described below:

$$p(h_{t_k}|C_{t_k} = c_j, C_{t_{k-1}} = c_i) = \frac{1}{\sigma_h\sqrt{2\pi}} \sum_{n=-\infty}^{\infty} \exp\left(-\frac{(\frac{\pi}{2} - \phi_{c_i,c_j} - h_{t_k} + 2\pi n)^2}{2{\sigma_h}^2}\right). \quad (4)$$

Here, ϕ_{c_i,c_j} represents the angle formed by the projection of the line connecting c_i to c_j onto the XY plane with the positive direction of the X-axis within the $[-\pi, \pi)$ radian range, and is measured counterclockwise from the positive direction of the X-axis; σ_h denotes the standard deviation of the platform's heading measurements.

$p(C_{t_k} = c_j|C_{t_{k-1}} = c_i)$ represents the probability distribution of transitioning from state c_i at time instant t_{k-1} to c_j at time instant t_k. This transition can be modeled by considering constraints such as door/wall limitations or the maximum permissible position change during a single time step as discussed in [34]. Alternatively, it can be treated as constant for all pairs c_i and c_j as proposed in [35]. To address ambiguities that may arise when two possible positions have the same posterior probability and are equidistant from

the single anchor, the developed positioning system models $p(C_{t_k} = c_j | C_{t_{k-1}} = c_i)$ as follows:

$$p(C_{t_k} = c_j | C_{t_{k-1}} = c_i) \propto \begin{cases} 1, & \text{if } |c_j - c_i| \leq s_{max} \cdot \Delta t_k, \\ 0, & \text{otherwise.} \end{cases} \tag{5}$$

Here, $|c_j - c_i|$ denotes the Euclidean distance between the hidden states c_j and c_i; s_{max} represents the platform's maximum achievable speed in m/s; Δt_k signifies the time interval between the instants t_k and t_{k-1} in s, i.e., $\Delta t_k = t_k - t_{k-1}$.

The denominator term $p(h_{t_k} | C_{t_{k-1}} = c_i)$ in (3) simplifies to $p(h_{t_k})$ as the platform's heading measurement h_{t_k} at time instant t_k is not dependent on c_i at time instant t_{k-1}.

D. MEASUREMENT UPDATE

During the measurement update, we compute the observation likelihood $p(d_{t_k}, a_{t_k} | C_{t_k} = c_j)$, representing the probability of observing d_{t_k} and a_{t_k} given the state c_j at time instant t_k. In the developed positioning system, the observation likelihood reflects the proximity between the platform and a particular grid cell on the map, considering the observed single-anchor distance and altitude measurements of the platform at time instant t_k. Given the single-anchor distance and altitude measurements of the platform are always independent of each other, we obtain

$$p(d_{t_k}, a_{t_k} | C_{t_k} = c_j) = p(d_{t_k} | C_{t_k} = c_j) p(a_{t_k} | C_{t_k} = c_j). \tag{6}$$

As the platform's distance from the single anchor cannot be negative, the observation likelihood for the platform's single-anchor distance measurement, denoted as $p(d_{t_k} | C_{t_k} = c_j)$, is computed using a truncated normal distribution as described below:

$$\begin{aligned} &p(d_{t_k} | C_{t_k} = c_j) \\ &= \frac{1}{\sigma_d \sqrt{2\pi}} \\ &\quad \times \exp\left(-\frac{(|c_j - (x_{anchor}, y_{anchor}, z_{anchor})| - d_{t_k})^2}{2{\sigma_d}^2}\right) \\ &\quad \cdot \frac{2}{1 - erf\left(\frac{-d_{t_k}}{\sigma_d \sqrt{2}}\right)} \end{aligned} \tag{7}$$

where $|c_j - (x_{anchor}, y_{anchor}, z_{anchor})|$ represents the Euclidean distance from the hidden state c_j to the known position coordinates of the single anchor $(x_{anchor}, y_{anchor}, z_{anchor})$; σ_d represents the standard deviation of the distance measurements between the platform and the single anchor; $erf()$ denotes the error function and defined as:

$$erf(\xi) = \frac{2}{\sqrt{\pi}} \int_0^{\xi} \exp(-\tau^2) d\tau. \tag{8}$$

Furthermore, the observation likelihood for the altitude measurement of the platform, $p(a_{t_k} | C_{t_k} = c_j)$, is computed using a normal distribution as described below:

$$p(a_{t_k} | C_{t_k} = c_j) = \frac{1}{\sigma_a \sqrt{2\pi}} \exp\left(-\frac{(c_j^z - a_{t_k})^2}{2{\sigma_a}^2}\right) \tag{9}$$

where c_j^z denotes the Z-axis coordinate of the hidden state c_j; σ_a represents the standard deviation of the platform's altitude measurements.

E. MAP MATCHING

After motion and measurement updates have been performed, the ensuing posterior probability distribution $p(C_{t_k} = c_j | h_{t_k}, d_{t_k}, a_{t_k})$ is obtained as follows:

$$\begin{aligned} p(C_{t_k} = c_j | h_{t_k}, d_{t_k}, a_{t_k}) &= p(d_{t_k} | C_{t_k} = c_j) \cdot p(a_{t_k} | C_{t_k} = c_j) \\ &\cdot \sum_{c_i} \left[\frac{p(h_{t_k} | C_{t_k} = c_j, C_{t_{k-1}} = c_i) \cdot p(C_{t_k} = c_j | C_{t_{k-1}} = c_i)}{p(h_{t_k})}\right. \\ &\left. \cdot p(C_{t_{k-1}} = c_i | h_{t_{k-1}}, d_{t_{k-1}}, a_{t_{k-1}})\right]. \end{aligned} \tag{10}$$

In (10), the probability $p(h_{t_k})$ can be treated as a constant term denoted by η. Given that $p(C_{t_k} = c_j | h_{t_k}, d_{t_k}, a_{t_k})$ is a probability distribution, η can be established through normalization at each recursion's conclusion. This ensures that the sum over the N possible positions $C_{t_k} = c_j$, where $j = 1, 2, \ldots, N$, results in 1. Consequently, the ensuing posterior probability distribution $p(C_{t_k} = c_j | h_{t_k}, d_{t_k}, a_{t_k})$ can be expressed as:

$$\begin{aligned} p(C_{t_k} = c_j | h_{t_k}, d_{t_k}, a_{t_k}) &= (1/\eta) \cdot p(d_{t_k} | C_{t_k} = c_j) \\ &\cdot p(a_{t_k} | C_{t_k} = c_j) \cdot \sum_{c_i} [p(h_{t_k} | C_{t_k} = c_j, C_{t_{k-1}} = c_i) \\ &\cdot p(C_{t_k} = c_j | C_{t_{k-1}} = c_i) \cdot p(C_{t_{k-1}} = c_i | h_{t_{k-1}}, d_{t_{k-1}}, a_{t_{k-1}})]. \end{aligned} \tag{11}$$

Finally, the platform's current position at time instant t_k can be inferred by assessing the most probable projection of the motion and measurement updates from (11) as:

$$\hat{C}_{t_k} = \underset{c_j \in \{c_1, c_2, \ldots, c_N\}}{\arg\max} \; p(C_{t_k} = c_j | h_{t_k}, d_{t_k}, a_{t_k}) \tag{12}$$

where $\hat{C}_{t_k}$ represents the estimated coordinates of the platform's position at the current time instant t_k.

III. SIMULATIONS

A. ILLUSTRATION OF THE BAYESIAN ESTIMATION STEPS IN 3D

The estimation steps of the recursive Bayesian estimator exploited by the developed positioning system are illustrated for one cycle in Fig. 4. Since the probability distributions described in the previous section assign 3D coordinate values to a real number (i.e., they are a function of three variables), there is no direct way to visualize them. Therefore, in this article, colors are used to represent the calculated probability values. Furthermore, slice surfaces within 3D are considered to depict the characteristics of the calculated probability distributions.

In this illustrative one cycle simulation, the single anchor is positioned at coordinates $(x_{anchor}, y_{anchor}, z_{anchor}) = (0, 0, 5)$. To aid visualization, we assume that the platform's initial position is precisely known to be $(-5, -5, 2)$.

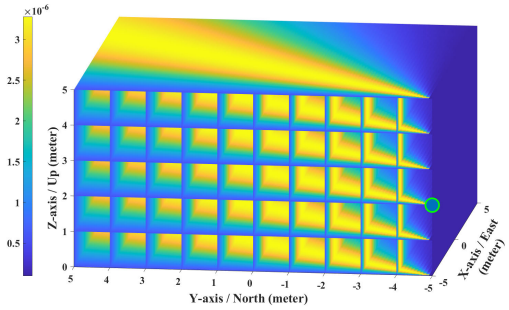

(a) Probability distribution representing the heading measurement of the platform, i.e., $p(h_{t_1}|C_{t_1}, C_{t_0}) \cdot p(C_{t_0}|h_{t_0}, d_{t_0}, a_{t_0})$.

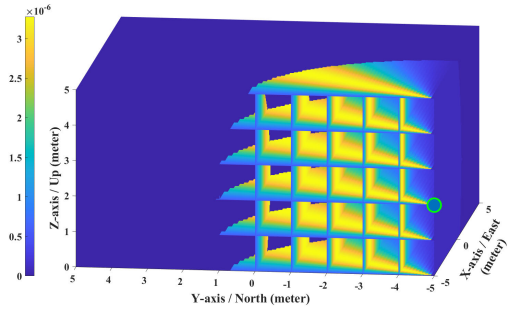

(b) Prior probability distribution after applying the maximum speed constraint, $p(C_{t_1}|h_{t_1}, d_{t_0}, a_{t_0})$.

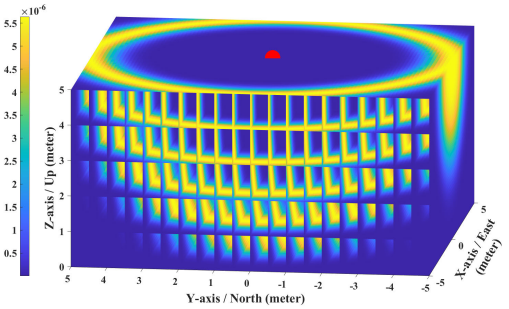

(c) Probability distribution characterizing the single-anchor distance measurement of the platform, i.e., $p(d_{t_1}|C_{t_1})$.

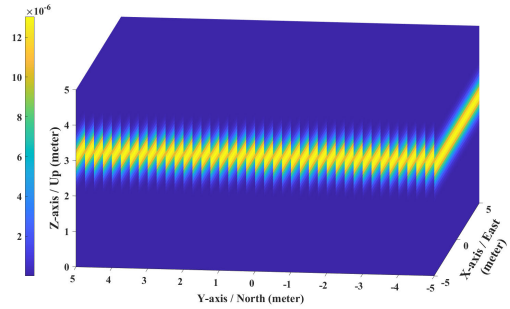

(d) Probability distribution characterizing the altitude measurement of the platform, i.e., $p(a_{t_1}|C_{t_1})$.

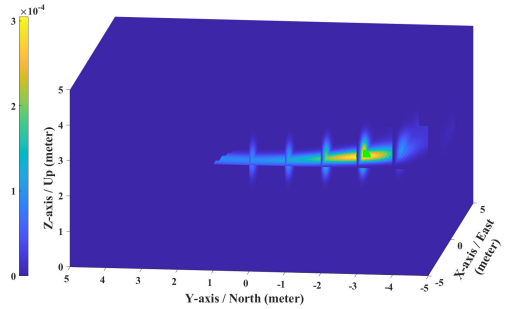

(e) Posterior probability distribution $p(C_{t_1}|h_{t_1}, d_{t_1}, a_{t_1})$ **providing the platform's position estimate at the current time instant** t_1.

FIGURE 4. The steps involved in the recursive Bayesian estimator utilized by the developed positioning system for one cycle.

Thus, the initial posterior probability distribution is provided as:

$$p(C_{t_0}|h_{t_0}, d_{t_0}, a_{t_0}) = \begin{cases} 1, & \text{if } C_{t_0} = (-5, -5, 2), \\ 0, & \text{otherwise.} \end{cases} \tag{13}$$

In the stage of motion update, a heading measurement $h_{t_1} = \pi/5$ radian with a standard deviation $\sigma_h = \pi/9$ radian is taken. This heading measurement and the initial posterior probability distribution in (13) give us the probability distribution $p(h_{t_1}|C_{t_1}, C_{t_0}) \cdot p(C_{t_0}|h_{t_0}, d_{t_0}, a_{t_0})$ as illustrated in Fig. 4a. Then, the time difference $\Delta t_1 = 1$ s between the instants t_1 and t_0, and the speed limit $s_{max} = 6$ m/s for the rectilinear motion of the platform are applied. Consequently, the prior probability distribution $p(C_{t_1}|h_{t_1}, d_{t_0}, a_{t_0})$ is obtained as illustrated in Fig. 4b. Note that the platform's initial position is denoted as a green circle in Fig. 4a and Fig. 4b.

In the stage of measurement update, the single-anchor distance and altitude measurements of the platform are taken as $d_{t_1} = 5$ m and $a_{t_1} = 3$ m with standard deviations $\sigma_d = 0.5$ m and $\sigma_a = 0.3$ m, respectively. Following this, the probability distributions $p(d_{t_1}|C_{t_1})$ and $p(a_{t_1}|C_{t_1})$ are obtained as illustrated in Fig. 4c and Fig. 4d, respectively. Note that the single anchor is denoted as a red point in Fig. 4c.

Ultimately, combining both the motion and measurement updates yields the resulting posterior probability distribution $p(C_{t_1}|h_{t_1}, d_{t_1}, a_{t_1})$. The platform's position estimate $\hat{C}_{t_1}$ at the current time instant t_1 is obtained by maximum a posteriori inference as illustrated in Fig. 4e. Note that the estimated position is denoted as a green point in Fig. 4e.

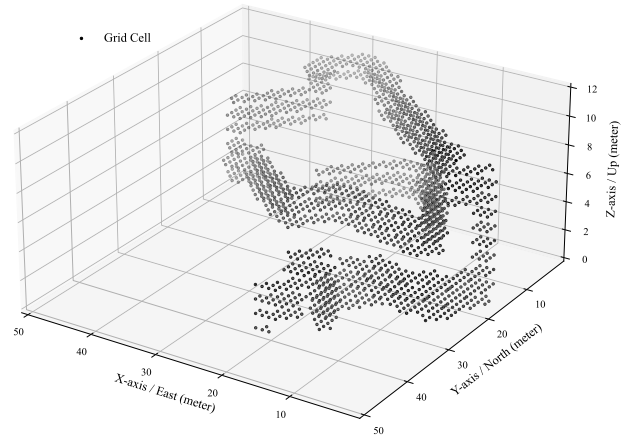

FIGURE 5. In the simulated scenario, a drone is assumed to be flying within a predescribed flying path with grid cells which are used as the hidden states of the dynamic naive Bayesian classifier.

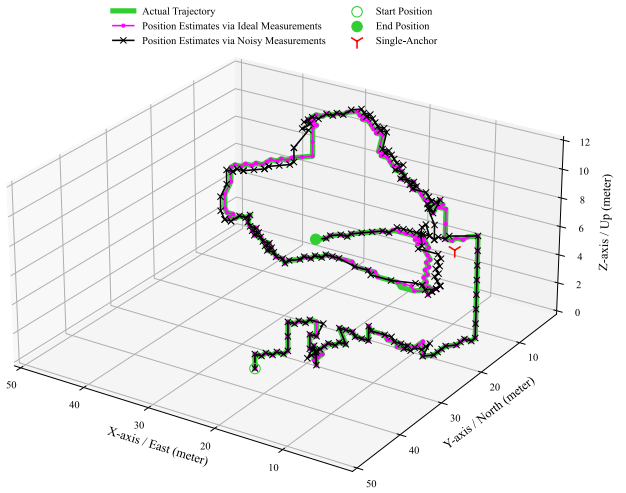

FIGURE 6. Simulation results in a 3D structured environment. It is assumed that the drone is outfitted with two distinct sets of sensors that provide ideal and noisy measurements at the same time instants.

B. SIMULATED SCENARIO FOR 3D POSITIONING

A scenario for a 3D positioning application in a structured environment is simulated to evaluate the performance of the developed positioning system. In the scenario, highly accurate 3D trajectory ground truth data recorded by a precise real-time kinematic (RTK) positioning system are borrowed from another research work (data from the folder "dataset1" between 30th and 60th seconds in [36]) where a flying drone is tracked by multiple cameras [37].

In the simulated scenario, the 3D environment of interest has 50 m x 50 m x 12 m volume. The drone is assumed to be flying within a predescribed flight path shown in Fig. 5, and the grids on this flight path are used as the hidden states of the DNBC.

Furthermore, it is assumed that the flying drone is outfitted with two distinct sets of sensors that take measurements at the same time instants t_k. The first sensor set on the drone includes ideal sensors providing noiseless measurements. On the other hand, the second sensor set on the drone includes nonideal sensors providing noisy heading, single-anchor distance, and altitude measurements with standard deviations $\sigma_h = \pi/36$ radian, $\sigma_d = 0.1$ m, and $\sigma_a = 0.1$ m, respectively. The drone flies with changing speeds on its trajectory, and the design parameter defining the maximum speed that the drone can reach is chosen as $s_{max} = 4$ m/s. It is assumed that the measurements are taken in every 0.03 s interval (that is, $\Delta t_k = 0.03$ s) for all k, and the single anchor is positioned at coordinates $(x_{anchor}, y_{anchor}, z_{anchor}) = (10, 10, 5)$.

The actual trajectory on which the drone flies (ground truth data from [36]) and the positions estimated by the developed positioning system via measurements acquired from two different sensor sets are shown in Fig. 6. As anticipated, position estimates based on ideal measurements perfectly correspond to the actual trajectory. Conversely, despite the sensors' relatively high error rates, position estimates derived from noisy measurements achieve errors lower than 3.16 m for 95% of the time with a mean of 0.98 m. The function of cumulative error distribution of simulation results in 3D structured environment is shown in Fig. 7.

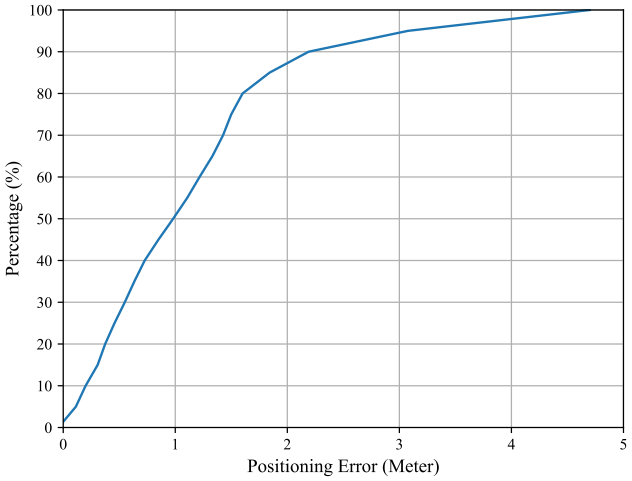

FIGURE 7. Cumulative error distribution for simulation results in a 3D structured environment.

IV. REAL-TIME APPLICATION RESULTS

A 2D real-time outdoor application was conducted to verify the effectiveness of the developed positioning system. The real-time application took place in a constrained area on The Ohio State University's campus, as depicted in Fig.8. To apply the developed system, first, a 2D map of the area of interest was created as shown in Fig. 9 using a local coordinate system and grid cells (10 cm distance between each other). Then, a UWB module [38] was placed in a position with known local coordinates (0.8,-21.5) as the single anchor, and a pedestrian carried out a walking experiment as shown in Fig. 10. The pedestrian was holding

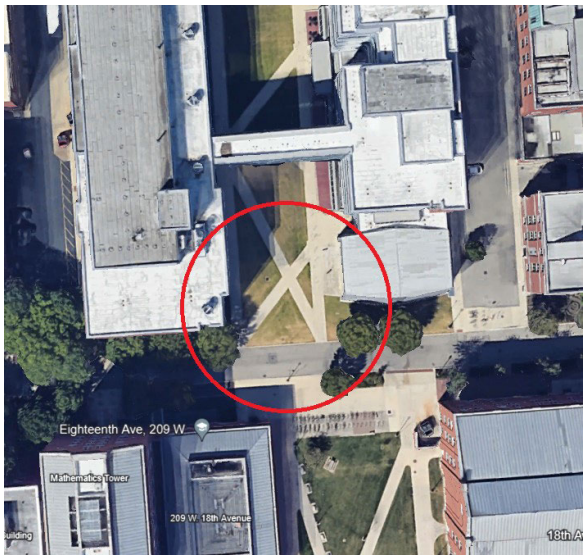

FIGURE 8. Real-time application took place in a constrained area on The Ohio State University's campus.

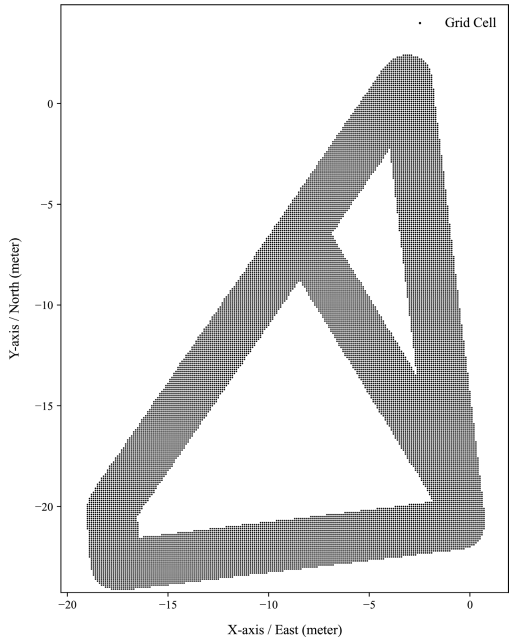

FIGURE 9. A 2D map of the area of interest was created using grid cells and a local coordinate system.

FIGURE 10. The single anchor was placed in a position with known local coordinates in the area of interest, and a pedestrian holding a sensor set carried out walking experiment for the real-time application.

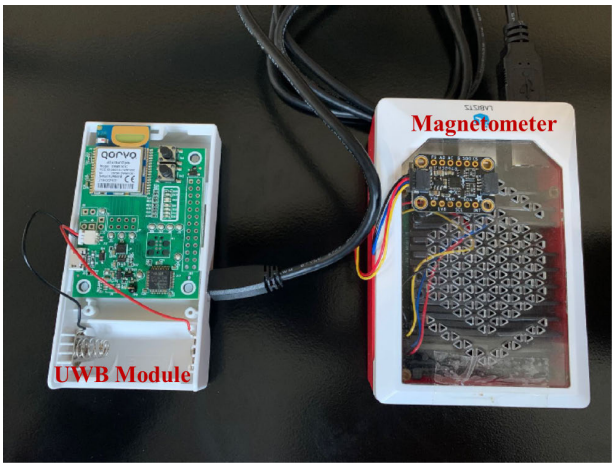

FIGURE 11. A sensor set containing a magnetometer and a UWB module was held by the pedestrian.

a set of sensors shown in Fig. 11, including a UWB module [38] and a triple-axis magnetometer [39] to collect the measurements of the single-anchor distance and the heading, respectively.

In the real-time application, the pedestrian started walking from the starting point and went along the numbered green lines from 1 to 7, respectively, in order to finish the walking where it was started and to have an 8-shaped trajectory as depicted in Fig. 12. The numbered green lines on the 8-shaped trajectory were used as ground truth in the real-time application.

The standard deviations for the measurements of the heading and single-anchor distance were taken as $\sigma_h = \pi/12$ radian and $\sigma_d = 0.3$ m, respectively. The pedestrian walked on the 8-shaped trajectory featuring speed changes, and the design parameter describing the maximum speed of the pedestrian was chosen as $s_{max} = 1.5$ m/s. Real-time heading and single-anchor distance measurements were synchronized and taken in every 0.5 s interval (that is, $\Delta t_k = 0.5$ s) for all k.

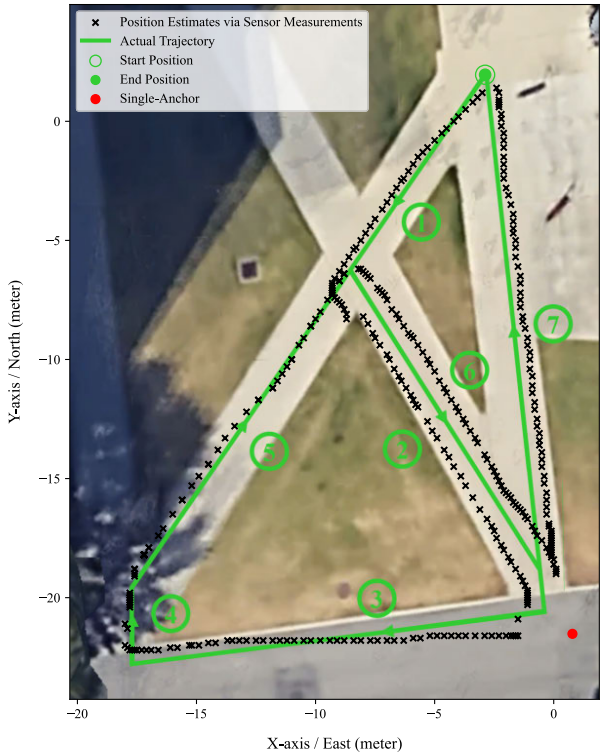

FIGURE 12. Real-time application results.

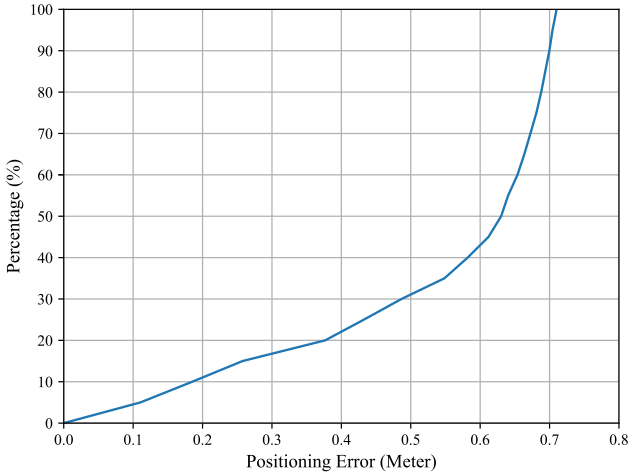

FIGURE 13. Cumulative error distribution for real-time application results.

Fig. 12 shows the positions estimated by the developed positioning system via measurements coming from the sensor set held by the pedestrian. The performance of the developed positioning system was evaluated by calculating the positioning errors which are the distances from the position estimates to the related green line on the 8-shaped trajectory. Since the sensor set was handheld, there were several factors that introduced noise into sensor measurements and thus had negative effect on the positioning performance (e.g., sensor orientation changes in unpredictable ways due to pedestrian's motion). Despite these challenges, the real-time performance of the developed system was with positioning errors lower than 0.7 m for 95% of the time with a mean of 0.52 m, which could be acceptable for the most real-time application scenarios in civilian and military areas. The function of cumulative error distribution of real-time application results is shown in Fig. 13.

V. CONCLUSION AND FUTURE WORK

In this article, a positioning system that can be used for 2D and 3D motion tracking has been developed. The methodology of the developed positioning system has been presented for 3D positioning using three types of measurements: heading, single-anchor distance, and altitude. However, for positioning applications that utilize 2D maps, the presented methodology can be easily adapted to provide a positioning solution using only two types of measurements: heading and projected single-anchor distance onto 2D plane. The developed system has originated from a dynamic naive Bayesian classifier, which is an extension of hidden Markov models, specifically designed for map matching.

The operational effectiveness of the developed positioning system has been demonstrated, showing promise for reliable and cost-efficient positioning solutions in both indoor and outdoor scenarios, particularly within constrained 2D or 3D environments. The potential benefits of applying the developed positioning system can be outlined as follows:

- The developed positioning system employs joint probability distributions, making it highly adaptable for the integration of diverse data types originating from various sensor technologies.
- The developed positioning system is scalable, allowing its utilization across multiple platforms simultaneously.
- The developed positioning system is extendable and applicable in vast areas of interest by incorporating multiple anchors.
- The developed positioning system leverages the heading, single-anchor distance, and altitude measurements of the platform that can be obtained from power- and cost-effective sensors to estimate the platform's current position through a dynamic naive Bayesian classifier map matching scheme. As a result, it is a size, weight, and power-cost (SWaP-C) oriented positioning system.

Future research will focus on performance comparison studies of the developed system with other SWaP-C oriented positioning systems. Moreover, we plan to carry out additional real-time applications of the developed positioning system in diverse usage scenarios within both 2D and 3D environments, utilizing various sensor sets with differing qualities.

ACKNOWLEDGMENT

This work was done while Serkan Zobar was with the Department of Civil, Environmental, and Geodetic Engineering, The Ohio State University as a visiting researcher.

REFERENCES

[1] J. Rantakokko, P. Händel, M. Fredholm, and F. Marsten-Eklöf, "User requirements for localization and tracking technology: A survey of mission-specific needs and constraints," in *Proc. Int. Conf. Indoor Positioning Indoor Navigat.*, Zurich, Switzerland, Sep. 2010, pp. 1–9, doi: 10.1109/IPIN.2010.5646765.

[2] A. Kumar, S. Kumar, P. Lal, P. Saikia, P. K. Srivastava, and G. P. Petropoulos, "Introduction to GPS/GNSS technology," in *GPS and GNSS Technology in Geosciences*, G. P. Petropoulos and P. K. Srivastava, Eds. Amsterdam, The Netherlands: Elsevier, 2021, ch. 1, pp. 3–20.

[3] E. D. Kaplan and C. J. Hegarty, *Understanding GPS/GNSS: Principles and Applications*. Boston, MA, USA: Artech House, 2017.

[4] D. A. Grejner-Brzezinska, C. K. Toth, T. Moore, J. F. Raquet, M. M. Miller, and A. Kealy, "Multisensor navigation systems: A remedy for GNSS vulnerabilities?" *Proc. IEEE*, vol. 104, no. 6, pp. 1339–1353, Jun. 2016, doi: 10.1109/JPROC.2016.2528538.

[5] T. Yang, A. Cabani, and H. Chafouk, "A survey of recent indoor localization scenarios and methodologies," *Sensors*, vol. 21, no. 23, p. 8086, Dec. 2021, doi: 10.3390/s21238086.

[6] S. Ghorpade, M. Zennaro, and B. Chaudhari, "Survey of localization for nodes: Approaches, challenges and open issues," *Future Internet*, vol. 13, no. 8, p. 210, Aug. 2021, doi: 10.3390/fi13080210.

[7] S. J. Hayward, K. van Lopik, C. Hinde, and A. A. West, "A survey of indoor location technologies, techniques and applications in industry," *Internet Things*, vol. 20, Nov. 2022, Art. no. 100608, doi: 10.1016/j.iot.2022.100608.

[8] D. Titterton and J. Weston, *Strapdown Inertial Navigation Technology*. Edison, NJ, USA: IET, 2004.

[9] C. Li, L. Mo, and D. Zhang, "Review on UHF RFID localization methods," *IEEE J. Radio Freq. Identificat.*, vol. 3, no. 4, pp. 205–215, Dec. 2019, doi: 10.1109/JRFID.2019.2924346.

[10] J. Yang, C. Poellabauer, P. Mitra, and C. Neubecker, "Beyond beaconing: Emerging applications and challenges of BLE," *Ad Hoc Netw.*, vol. 97, Feb. 2020, Art. no. 102015, doi: 10.1016/j.adhoc.2019.102015.

[11] X. Tong, H. Li, X. Tian, and X. Wang, "Wi-Fi localization enabling self-calibration," *IEEE/ACM Trans. Netw.*, vol. 29, no. 2, Apr. 2021, Art. no. 904917, doi: 10.1109/TNET.2021.3051998.

[12] O. N. Güneş, E. Aksoy, and S. Zobar, "A multi-dimensional scaling application with ultra-wideband and ultrasound ranging," in *Proc. 28th Signal Process. Commun. Appl. Conf. (SIU)*, Oct. 2020, pp. 1–4, doi: 10.1109/SIU49456.2020.9302428.

[13] S. Zobar and E. Aksoy, "An application of relative node positioning using ultra-wideband distance estimates," presented at the NATO SET-275 Symp. Cooperat. Navigat. GNSS Degraded Denied Environ., 2021. Accessed: Jan. 20, 2024. [Online]. Available: https://www.sto.nato.int/publications/STO%20Meeting%20Proceedings/STO-MP-SET-275/MP-SET-275-03.pdf

[14] M. Aernouts, T. Janssen, R. Berkvens, and M. Weyn, "LoRa localization: With GNSS or without?" *IEEE Internet Things Mag.*, vol. 5, no. 3, pp. 152–157, Sep. 2022, doi: 10.1109/IOTM.001.2200019.

[15] S. Sophia, B. M. Shankar, K. Akshya, AR. C. Arunachalam, V. T. Y. Avanthika, and S. Deepak, "Bluetooth low energy based indoor positioning system using ESP32," in *Proc. 3rd Int. Conf. Inventive Res. Comput. Appl. (ICIRCA)*, Sep. 2021, pp. 1698–1702, doi: 10.1109/ICIRCA51532.2021.9544975.

[16] S. Güney, A. Erdogan, M. Aktas, and M. Ergün, "Wi-Fi based indoor positioning system with using deep neural network," in *Proc. 43rd Int. Conf. Telecommun. Signal Process. (TSP)*, Jul. 2020, pp. 225–228, doi: 10.1109/TSP49548.2020.9163548.

[17] Qorvo. *DW1000 Product Datasheet*. Accessed: Jan. 20, 2024. [Online]. Available: https://www.qorvo.com/products/p/DW1000

[18] K.-H. Lam, C.-C. Cheung, and W.-C. Lee, "RSSI-based LoRa localization systems for large-scale indoor and outdoor environments," *IEEE Trans. Veh. Technol.*, vol. 68, no. 12, pp. 11778–11791, Dec. 2019, doi: 10.1109/TVT.2019.2940272.

[19] S. Zobar and M. Çiydem, "UDOKS project: Development of a pedestrian navigation system with multiple integrated sensors," presented at the IEEE 12th Int. Conf. Indoor Positioning Indoor Navigat. (IPIN), Sep. 2022, Beijing, China. Accessed: Jan. 20, 2024. [Online]. Available: https://ceur-ws.org/Vol-3248/paper16.pdf

[20] X. Yun, J. Calusdian, E. R. Bachmann, and R. B. McGhee, "Estimation of human foot motion during normal walking using inertial and magnetic sensor measurements," *IEEE Trans. Instrum. Meas.*, vol. 61, no. 7, pp. 2059–2072, Jul. 2012, doi: 10.1109/TIM.2011.2179830.

[21] T. Gädeke, J. Schmid, M. Zahnlecker, W. Stork, and K. D. Müller-Glaser, "Smartphone pedestrian navigation by foot-IMU sensor fusion," in *Proc. Ubiquitous Positioning, Indoor Navigat., Location Based Service (UPINLBS)*, Oct. 2012, pp. 1–8, doi: 10.1109/UPINLBS.2012.6409787.

[22] Z.-A. Deng, Y. Hu, J. Yu, and Z. Na, "Extended Kalman filter for real time indoor localization by fusing WiFi and smartphone inertial sensors," *Micromachines*, vol. 6, no. 4, pp. 523–543, Apr. 2015, doi: 10.3390/mi6040523.

[23] R. Ali, R. Liu, A. Nayyar, B. Qureshi, and Z. Cao, "Tightly coupling fusion of UWB ranging and IMU pedestrian dead reckoning for indoor localization," *IEEE Access*, vol. 9, pp. 164206–164222, 2021, doi: 10.1109/ACCESS.2021.3132645.

[24] Y. Wu, P. Chen, F. Gu, X. Zheng, and J. Shang, "HTrack: An efficient heading-aided map matching for indoor localization and tracking," *IEEE Sensors J.*, vol. 19, no. 8, pp. 3100–3110, Apr. 2019, doi: 10.1109/JSEN.2019.2891313.

[25] V. Guimarães, L. Castro, S. Carneiro, M. Monteiro, T. Rocha, M. Barandas, J. Machado, M. Vasconcelos, H. Gamboa, and D. Elias, "A motion tracking solution for indoor localization using smartphones," in *Proc. Int. Conf. Indoor Positioning Indoor Navigat. (IPIN)*, Oct. 2016, pp. 1–8, doi: 10.1109/IPIN.2016.7743680.

[26] M. Klepal, Widyawan, and S. Beauregard, "A backtracking particle filter for fusing building plans with PDR displacement estimates," in *Proc. 5th Workshop Positioning, Navigat. Commun.*, Mar. 2008, Art. no. 207212, doi: 10.1109/wpnc.2008.4510376.

[27] A. Perttula, H. Leppäkoski, M. Kirkko-Jaakkola, P. Davidson, J. Collin, and J. Takala, "Distributed indoor positioning system with inertial measurements and map matching," *IEEE Trans. Instrum. Meas.*, vol. 63, no. 11, pp. 2682–2695, Nov. 2014, doi: 10.1109/TIM.2014.2313951.

[28] Y. Gu, Q. Song, Y. Li, and M. Ma, "Foot-mounted pedestrian navigation based on particle filter with an adaptive weight updating strategy," *J. Navigat.*, vol. 68, no. 1, pp. 23–38, Jan. 2015, doi: 10.1017/s0373463314000496.

[29] R. Mahony, T. Hamel, and J.-M. Pflimlin, "Nonlinear complementary filters on the special orthogonal group," *IEEE Trans. Autom. Control*, vol. 53, no. 5, pp. 1203–1218, Jun. 2008, doi: 10.1109/TAC.2008.923738.

[30] M. T. Koroglu, M. Korkmaz, A. Yilmaz, and A. Durdu, "Multiple hypothesis testing approach to pedestrian INS with map-matching," in *Proc. Int. Conf. Indoor Positioning Indoor Navigat. (IPIN)*, Sep. 2019, pp. 1–8, doi: 10.1109/IPIN.2019.8911787.

[31] S. Zobar, M. Çiydem, Ö. Salor, C. K. Toth, and A. Yilmaz, "2D-HASAP: Two-dimensional heading-aided single-anchor positioning via hidden Markov model map-matching," in *Proc. IEEE Symp. Sensor Data Fusion Int. Conf. Multisensor Fusion Integr. (SDF-MFI)*, Bonn, Germany, Nov. 2023, pp. 1–6, doi: 10.1109/sdf-mfi59545.2023.10361293.

[32] M. A. Palacios-Alonso, C. A. Brizuela, and L. E. Sucar, "Evolutionary learning of dynamic Naive Bayesian classifiers," *J. Automated Reasoning*, vol. 45, no. 1, pp. 21–37, Jun. 2010, doi: 10.1007/s10817-009-9130-0.

[33] Z. Ghahramani, "An introduction to hidden Markov models and Bayesian networks," *Int. J. Pattern Recognit. Artif. Intell.*, vol. 15, no. 1, pp. 9–42, Feb. 2001.

[34] S. Lamy-Perbal, N. Guénard, M. Boukallel, and A. Landragin-Frassati, "A HMM map-matching approach enhancing indoor positioning performances of an inertial measurement system," in *Proc. Int. Conf. Indoor Positioning Indoor Navigat. (IPIN)*, Oct. 2015, pp. 1–4, doi: 10.1109/IPIN.2015.7346774.

[35] J. Seitz, J. Jahn, J. G. Boronat, T. Vaupel, S. Meyer, and J. Thielecke, "A hidden Markov model for urban navigation based on fingerprinting and pedestrian dead reckoning," in *Proc. 13th Int. Conf. Inf. Fusion*, Jul. 2010, pp. 1–8, doi: 10.1109/ICIF.2010.5712025.

[36] *Drone Tracking Datasets*. Accessed: Jan. 20, 2024. [Online]. Available: https://github.com/CenekAlbl/drone-tracking-datasets?tab=readme-ov-file

[37] J. Li, J. Murray, D. Ismaili, K. Schindler, and C. Albl, "Reconstruction of 3D flight trajectories from ad-hoc camera networks," in *Proc. IEEE/RSJ Int. Conf. Intell. Robots Syst. (IROS)*, Las Vegas, NV, USA, Oct. 2020, pp. 1621–1628, doi: 10.1109/IROS45743.2020.9341479.

[38] Qorvo. *DWM1000*. Accessed: Jan. 20, 2024. [Online]. Available: https://www.qorvo.com/products/p/DWM1000
[39] *TDK. ICM-20948*. Accessed: Jan. 20, 2024. [Online]. Available: https://invensense.tdk.com/products/motion-tracking/9-axis/icm-20948/

SERKAN ZOBAR was born in Enez, Türkiye. He received the B.Sc. and M.Sc. degrees in electronics engineering from Hacettepe University, Ankara, Türkiye, in 2001 and 2004, respectively. He is currently pursuing the Ph.D. degree in electronics engineering with Gazi University, Ankara.

From 2001 to 2010, he was with the Department of Electrical and Electronics Engineering, Hacettepe University, as a Research Assistant. From 2007 to 2008, he was with the Department of Engineering Cybernetics, Norwegian University of Science and Technology, Trondheim, Norway, as a Visiting Researcher. From 2010 to 2023, he was with Aselsan Inc., Ankara, as a Lead Design Engineer. From 2022 to 2023, he was with the Department of Civil, Environmental, and Geodetic Engineering, The Ohio State University, Columbus, OH, USA, as a Visiting Researcher. His research interests include positioning, navigation and timing (PNT) systems, sensor fusion, and system modeling and identification.

Mr. Zobar is a recipient of the Sensors and Electronics Technology Panel Excellence Award from NATO Science and Technology Organization.

MEHMET CIYDEM was born in Ankara, Türkiye. He received the B.Sc., M.Sc., and Ph.D. degrees (Hons.) in electrical engineering from Middle East Technical University, Ankara, in 1993, 1995, and 2004, respectively.

After working in defense industry (Aselsan, Havelsan, TAI) for many years, he founded Engitek Ltd. company, where he is currently the President. He is also one of the Founders and a Board Member of Communication Technologies Cluster, Türkiye. He is a Professor of electromagnetics, communications, and lectures occasionally in several universities (Bilkent University, Gazi University, Karatay University, Hacettepe University, and Army War Academy). His research interests include electromagnetics, antennas, RF/microwave engineering, radar, communication systems, and mobile communications networks.

ÖZGÜL SALOR (Senior Member, IEEE) received the B.Sc., M.Sc., and Ph.D. degrees in electrical and electronics engineering from Middle East Technical University, Ankara, Türkiye, in 1997, 1999, and 2005, respectively.

From 2001 to 2003, she was a Professional Researcher with the Center for Spoken Language Research, University of Colorado, Boulder, CO, USA. From 2006 to 2012, she was with the Power Electronics Department, Space Technologies Research Institute, Scientific and Technological Research Council of Türkiye. Since 2012, she has been a Professor with the Department of Electrical and Electronics Engineering, Gazi University, Ankara. Since August 2019, she has been with Kyrgyz-Turkish Manas University, Kyrgyzstan to start the new Department of Electrical and Electronics Engineering. Her research interests include machine learning techniques and signal processing for power quality analysis.

Dr. Salor was a recipient of the Outstanding Paper Award and Certificate of Recognition Award from the Metal Industry Committee of the IEEE Industry Applications Society, in 2009, 2015, and 2022 and Meritorious Paper Award of MIC, in 2013 and 2019.

JIYONG KWAG was born in Seoul, South Korea. He received the B.Sc. degree in computer and information science from The Ohio State University, Columbus, OH, USA, in 2023, where he is currently pursuing the Ph.D. degree in civil, environmental, and geodetic engineering.

In 2023, he was an Undergraduate Research Assistant with the Department of Civil, Environmental, and Geodetic Engineering, contributing to the Single-Anchor Localization Project, The Ohio State University. He also worked with the Department of Computer Science and Engineering on the Multiday Stock Prediction Project, The Ohio State University. Since 2024, he has been a Graduate Research Assistant with the Center for Automotive Research (CAR), The Ohio State University. His research interests include GNSS-denied positioning, sensor fusion, and high-definition (HD) map generation.

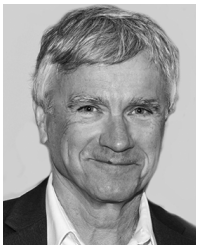

CHARLES K. TOTH (Life Senior Member, IEEE) received the M.Sc. degree in electrical engineering and the Ph.D. degree in electrical engineering and geoinformation sciences from the Technical University of Budapest, Budapest, Hungary, in 1977 and 1980, respectively.

He was a Senior Research Scientist with the Center for Mapping, having 30 years of research experience, The Ohio State University, Columbus, OH, USA. He is currently a Research Professor with the Department of Civil, Environmental, and Geodetic Engineering. He has authored or coauthored more than 400 peer-reviewed journal and proceedings articles. His research interests include spatial information systems, LiDAR, high-resolution imaging, surface extraction, modeling, integration, and calibration of multisensor systems, multisensor geospatial data acquisition systems, 2-D/3-D signal processing, and mobile mapping technologies.

Dr. Toth is a Fellow of American Society of Photogrammetry and Remote Sensing (ASPRS), a Fellow of the Institute of Navigation, a Fellow of the International Society of Photogrammetry and Remote Sensing, and an ASPRS Certified Photogrammetrist. He was a recipient of the 2005 and 2015 United States Geospatial Information Foundation Academic Research Awards, the 2018 ASPRS Outstanding Service Award, the 2016 ISPRS Schwidefsky Medal, the 2013 OSU College of Engineering Lumley Research Award, the 2009 ASPRS Photogrammetric Award (Fairchild), and many ASPRS and Institute of Navigation Best Paper Awards. He is the past President of the ASPRS. He is the Vice-President of the International Society of Photogrammetry and Remote Sensing.

ALPER YILMAZ (Senior Member, IEEE) is currently a Professor of geodetic engineering with the Civil Engineering Department and the Computer Science and Engineering Department, The Ohio State University, Columbus, OH, USA. His research interests include 2D and 3D image and video understanding from image streams.

He is an Active Member of the Association for Computing Machinery and the American Society for Photogrammetry and Remote Sensing Professional Societies. He was a recipient of the Turkish Informatics Foundation High Academic Performance Award, in 1999; the two Graduate Merit Fellowships from UCF, in 2000 and 2001; the Hillman Award for Excellence in Research from UCF, in 2003; the Duane Brown Photogrammetry Award from OSU, in 2008; and the Lumley Research Award from the College of Engineering, OSU, in 2012. He is also chairing the International Society for Photogrammetry and Remote Sensing Working Group on Image Sequence Analysis. He organized a number of conferences and workshops on computer vision and photogrammetry fields. He served as an Associate Editor for *Machine Vision and Applications* journal, from 2006 to 2011.